Available online at www.sciencedirect.com
ScienceDirect
Journal of Power Sources 172 (2007) 604–612
JOURNAL OF POWER SOURCES
www.elsevier.com/locate/jpowsour

# Sorbitol-plasticized chitosan/zeolite hybrid membrane for direct methanol fuel cell

Weikang Yuan [a], Hong Wu [a], Bin Zheng [a], Xiaohong Zheng [a], Zhongyi Jiang [a,*], Xiaopeng Hao [b], Baoyi Wang [b]

[a] *School of Chemical Engineering and Technology, Tianjin University, Tianjin 300072, PR China*
[b] *Key Laboratory of Nuclear Analysis Techniques, Institute of High Energy Physics, Chinese Academy of Sciences, Beijing 100049, China*

Received 21 March 2007; received in revised form 12 May 2007; accepted 15 May 2007
Available online 18 May 2007

**Abstract**

Organic–inorganic hybrid membranes, as promising direct methanol fuel cell membranes, have become a research focus in recent years. Wherein interfacial morphology, greatly influenced by the polymer chain flexibility and interfacial stress generated during membrane formation, is a critical determinant of efficient suppression of methanol crossover. In this study, a novel and feasible approach for rational fabrication of organic/inorganic hybrid direct methanol fuel cell (DMFC) membrane is tentatively explored. By adding plasticizer in the membrane casting solution and/or elevating solvent evaporation temperature during membrane fabrication, the glass transition temperature ($T_g$) and crystallinity of the chitosan/zeolite hybrid membrane are both remarkably decreased. In particular, the interface voids are substantially eliminated, generating a more desirable interfacial morphology and consequently leading to an improved performance in suppressing methanol crossover. The chitosan/mordenite/sorbitol hybrid membrane prepared with 30 wt% of sorbitol and 15 wt% of mordenite exhibits a 44% reduction in methanol permeability compared with chitosan control membrane. The variation of methanol permeability with mordenite and sorbital content is tentatively elucidated by the change of free volume cavity size in the membrane determined by positron annihilation lifetime spectroscopy (PALS) measurements.


*Keywords:* DMFC; Organic–inorganic hybrid membrane; Plasticizer; Interfacial morphology; Methanol crossover

## 1. Introduction

Direct methanol fuel cell (DMFC), as an efficient and clean energy generator, provides an attractive alternative to the rechargeable battery in portable electronic devices [1]. Among the factors limiting the practical application of DMFC, methanol crossover through the polymer electrolyte membranes (PEMs), such as the most-commonly used Nafion membrane, constitutes one of the most concerned issues [2]. Synthesis of new types of polymer [3–7] and organic–inorganic hybrid materials [8–14] represent the prevailing strategies to reduce or inhibit methanol crossover in the development of DMFC-oriented membrane.

Often referred to the next generation membrane [15–17], organic–inorganic hybrid membrane has attracted peculiar attention as a promising DMFC membrane alternative, due to the possibility of not only combining the favorable properties from both organic and inorganic worlds but also creating entirely new compositions with truly unique properties [18]. However, how to obtain a desirable interfacial morphology, which is a critical determinant of permeation performance, is an important research issue in organic–inorganic hybrid membrane realm [19].

The interfacial morphology of hybrid membranes is tightly associated with different preparation techniques. So far, two strategies for incorporating inorganic species into polymer matrix have been proposed: (i) in situ formation of inorganic particles within polymer matrix through sol–gel reaction [17,20–23] or crystallization [22]. It is claimed that the nano-sized inorganic particles and uniform dispersion can be achieved by this strategy and, in some cases, the covalent bonds formed between organic and inorganic components may allow delicate tailoring of the interfacial properties [23]. However, the diffi-

* Corresponding author. Tel.: +86 22 27892143; fax: +86 22 27892143.
*E-mail address:* zhyjiang@tju.edu.cn (Z. Jiang).

0378-7753/$ – see front matter © 2007 Elsevier B.V. All rights reserved.
doi:10.1016/j.jpowsour.2007.05.040

cult control of hydrolysis and condensation reaction in sol–gel processes complicates membrane preparation and limits polymer selection. (ii) Physical mixing of organic solutions with inorganic fillers followed by simple casting [8-10,12,23-28]. In this strategy, organic and inorganic components usually interact through weak hydrogen bonding, van der Waals contacts and/or electrostatic forces [29]. The interphase in the membranes, which is a domain extending from the inorganic filler surface to the organic bulk, will dramatically impact the overall membrane properties [30,31].

For a given polymer and inorganic filler, stress generated at the interface during membrane preparation process is believed to determine whether an interphase forms and to what extent [19]. Koros [19,30] validated that forming membranes by maintaining the polymer in rubbery state is an effective strategy for obtaining an ideal interphase, but it obviously confronts a great challenge to achieve the rubbery state under the boiling point temperature of solvent for most of the glassy polymeric membrane materials. Whereas stress tends to be large for rigid polymers and lower stress promotes ideal interfacial morphology [30], decreasing the rigidity or to say increasing the flexibility of polymer chains during membrane formation while the polymer is still kept in glassy state, seems a rational and feasible approach [32].

For organic–inorganic DMFC hybrid membranes, the control of interfacial morphology (such as void size) is essential to reducing the methanol crossover because of the close kinetic diameters of methanol and water molecules (methanol: 0.380 nm, water: 0.264 nm [33]) and the determinant role of interfacial transport property in the overall transport process [19]. The addition of inorganic particles will induce the additional stress and influence the interfacial morphology in the following two aspects [34]. (1) Matrix rigidification. A rigidified polymer region around the inorganic fillers is formed, which can be indicated either by an increased $T_g$ or by an appearance of the second $T_g$ of the polymer. Due to the lower chain segmental mobility of polymer, this compressed region shows reduced permeability [35,36]. (2) Voids at interface. This is the most common non-ideal interfacial morphology for glassy polymers [19], and the non-selective voids considerably enhanced methanol permeation. Because the stress is ascribed to polymer chain rigidity, tailoring the chain rigidity of glassy polymer to acquire optimum interfacial morphology and improved methanol permeability is obviously crucial.

The objective of this study is to reduce the methanol crossover through polymer-zeolite hybrid membrane by tailoring the interfacial morphology through homogenous incorporation of sorbitol as a plasticizer and appropriate control of membrane formation temperature. Considering the distinct advantages as an excellent alcohol barrier [37,38] and ion-conductive material [39–41], chitosan (CS) was employed as the bulk polymer. Zeolites were chosen as inorganic filler because their ordered structure and regular pore size ensure the size-selective and shape-selective separations, and mordenite was chosen due to its tunable hydrophilicity, appropriate pore size (0.4 nm), acceptable proton conductivity, excellent stabilities and facile modification [42–44]. Sorbitol, a polyol with a boiling point of 295 °C and $T_g$ of −7 °C [45], was used as a plasticizer to increase the flexibility of chitosan, because its effective plasticizing function has been validated by many researchers [46,47].

Sorbitol-plasticized CS/mordenite hybrid membranes were prepared under 60 °C, and the intermolecular interaction, cross-section morphology, glass transition temperature, crystalline structure and free volume property of the membranes were systematically characterized. Water/methanol uptake and methanol permeability were briefly evaluated, and the correlation between interfacial morphologies and methanol permeability was tentatively revealed.

## 2. Experimental

### 2.1. Materials

CS (Zhejiang Golden-shell Biochemical Co., Ltd.), with a degree of deacetylation of 91%, was used as received. Mordenite (CBV 10A) with a Si/Al of 6.5 was purchased from Zeolite International, and with a mortar and pestle, it was dispersed using ethanol and sorbitol as dispersant before use. D-Sorbitol, acetic acid, sulfuric acid and methanol were all purchased locally. De-ionized water was used throughout the study.

### 2.2. Membrane preparation

CS/mordenite hybrid membrane: 3 g CS was dissolved in 150 mL 2 wt.% acetic acid solution at 80 °C, and then a desired amount of mordenite was added. The solution was dispersed under ultrasonic for 1 h and followed by stirring for another 3 h. After filtration and degasification, the resulting homogenous and bubble-free solution was cast onto a clean glass plate and the solvent was allowed to evaporate at 25 °C. The membrane was then cross-linked in 2 mol $L^{-1}$ $H_2SO_4$ for 24 h and rinsed with de-ionized water, followed by drying in vacuum.

Sorbitol-plasticized CS membrane: CS was dissolved in acetic acid solution containing certain amount of sorbitol. The following procedures were same as CS/mordenite hybrid membranes except the addition of mordenite.

Sorbitol-plasticized CS/mordenite hybrid membrane was prepared in a similar procedure as sorbitol-plasticized CS membrane except that mordenite was added and the solvent was evaporated at 25 °C or 60 °C.

CS control membrane was prepared in exactly the same way as above without adding mordenite and sorbitol.

For simplicity, CS control membrane, CS/mordenite hybrid membranes, sorbitol-plasticized CS membranes and sorbitol-plasticized CS/mordenite hybrid membranes are designated as CS-T, CS/M(X)-T, CS/S(Y)-T and CS/M(X)/S(Y)-T, respectively, where $X$ ($X$ = 5, 10, 15 or 20) and $Y$ ($Y$ = 20, 30 or 40) indicate the weight percentage of mordenite to CS and the weight percentage of sorbitol to CS, and $T$ ($T$ = 25 or 60) is the membrane preparation temperature. In plasticized membranes, sorbitol is supposed to be completely removed during the post-treatment steps because of its large solubility in water

(235 g/100 mL water). The thicknesses of all the membranes are in the range of 50–80 μm.

### 2.3. Membrane characterization

The FTIR spectra were recorded on a Nicolet, 5DX instrument (resolution 4 $cm^{-1}$) to characterize surface groups of mordenite and the chemical structure of interface. The pressed disks of pure mordenite powders were activated "in situ" in the IR cell by outgassing at 773 K before measurement.

The sample morphology was observed by SEM (Philips XL30ESEM) after being coated with gold. For membrane sample, it was first fractured in liquid nitrogen and then coated with gold.

The crystalline structure of mordenite and membrane was investigated using a X-ray diffractometer (Rigaku D/max2500v/pc, CuK 40 kV, 200 mA) in the range of 5–45° at the speed of 2° $min^{-1}$. The peak position and area were extracted using MDI jade5 software, and then chitosan crystallinity and overall crystallinity were calculated by Eqs. (1) and (2):

$$\text{chitosan crystallinity} = \frac{\text{total area of CS crystalline peaks}}{\text{total area of CS peaks}} \times 100\% \quad (1)$$

$$\text{overall crystallinity} = \frac{\text{total area of crystalline peaks}}{\text{total area of all peaks}} \times 100\% \quad (2)$$

The $T_g$ of the membrane was measured using a differential scanning calorimeter (Perkin-Elmer PYRIS Diamond) calibrated using indium and all the measurements were carried out under a nitrogen atmosphere. The amount of sample used was around 8 mg. In the first heating run, the sample was heated from 0 °C to 110 °C and held on for 20 min, then quenched to 0 °C and held on for 5 min. In the second heating run, the sample was heated from 0 °C to 240 °C and the $T_g$ was obtained from the second heating run curve. The heating and cooling rates were both set at 10 °C $min^{-1}$.

PALS measurements were carried out using an EG& GORTEC fast-slow coincidence system with a resolution of 190 ps (full width at half maximum). A $5 \times 10^5$ Bq source of 22Na was sandwiched between two pieces of sample. The measurements of the positron annihilation were performed at room temperature and the results were analyzed with POSITRONFIT-88 program in which variances of fit ($o$) between 0.987 and 1.109 were obtained.

### 2.4. Water/methanol uptake measurements

The water/methanol uptake of the membranes was determined by soaking pre-weighed membrane sample ($W_{dry}$) in de-ionized water or 12 mol $L^{-1}$ methanol/water solution. The sample was wiped to remove the surface water and weighed after different time intervals until a constant weight ($W_{wet}$) was achieved. The final uptake value was the average of three measurements with an error within ±4.6% and determined by Eq. (3):

$$\%\text{Uptake} = \frac{(W_{wet} - W_{dry})}{W_{dry}} \times 100\% \quad (3)$$

### 2.5. Methanol permeability measurements

Methanol permeability was measured with a diffusion cell [8]. The diffusion cell consisting of two compartments was separated by vertical fixed membrane that had been pre-hydrated in de-ionized water for 48 h. One compartment was filled with de-ionized water and the other with methanol/water solution (12 mol $L^{-1}$). The solution in the two compartments was stirred continuously during testing. Prior to measurement, membranes were. The concentration of methanol in the receipt compartment was determined using a gas chromatography (Agilent 6820) equipped with a TCD detector and a DB624 column. $S$ was the slope of the line of concentration versus time and the methanol permeability ($P$, $cm^2$ $s^{-1}$) was calculated by Eq. (4).

$$P = \frac{SV_B L}{AC_{A0}} \quad (4)$$

Herein, $V_B$ is the volume of the receipt compartment; $C_{A0}$ the concentration of feed; $A$ and $L$ are the membrane area and thickness, respectively. Each sample was measured three times and the average value was calculated with an error within ±4.3%.

## 3. Results and discussion

### 3.1. FTIR study

FTIR spectra suggest that hydroxyl groups exist on the mordenite surface and there is weak hydrogen bonding between mordenite and chitosan. Fig. 1(a) shows the FTIR spectra of mordenite activated at 773 K in a vacuum. Two bands can be observed in the OH stretching region: the first at 3739 $cm^{-1}$ associated with the terminal silanol groups on mordenite surface, and the second one at 3598 $cm^{-1}$ assigned to the bridging Si–OH–Al groups [48]. In Fig. 1(b), the shifts of amide I band (1648 $cm^{-1}$) and amide II band (1565 $cm^{-1}$) in chitosan molecule toward lower wavenumbers (1640 and 1553 $cm^{-1}$, respectively) should arise from the hydrogen bonds between surface hydroxyl groups of mordenite and amino groups in chitosan molecules.

### 3.2. SEM study

The mordenite particle and miscibility of organic and inorganic phase were investigated by SEM. Fig. 2(a) shows dispersed mordenite particle with an approximate size of 100 nm. According to Fig. 2(b and c), mordenite aggregation and void formation become more obvious with the increase of mordenite content. However, after addition of sorbitol, reduction in mordenite aggregation and void formation can be clearly observed from Fig. 2(b and d). At higher amplification (Fig. 2e), homogeneous dispersion of mordenite in CS matrix and excellent compatibil-

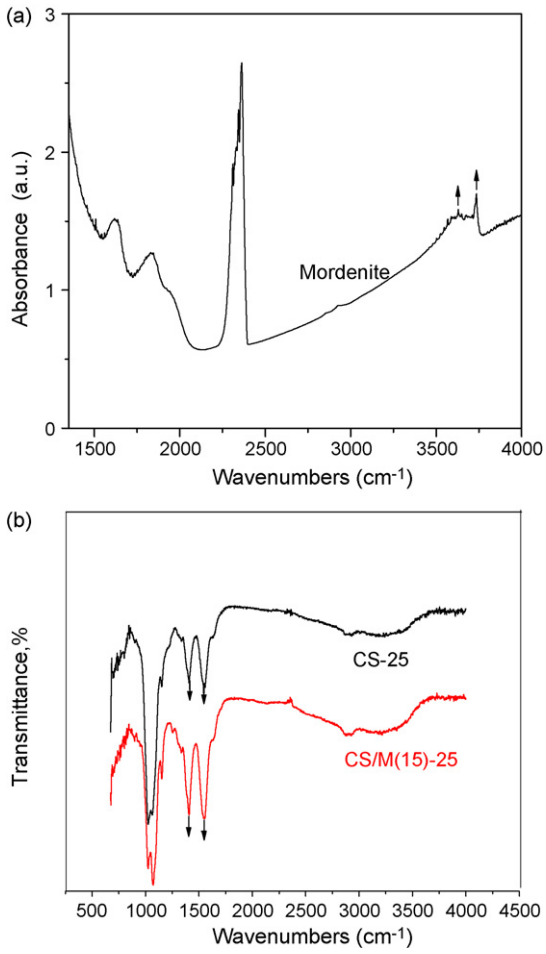


Fig. 1. FTIR spectra: (a) mordenite activated at 773 K under vacuum conditions; (b) CS-25 and CS/M (15)-25 membranes.

ity can be clearly observed in CS/M(15)/S(30)-25 membrane. Fig. 2(e and f) suggest that elevating membrane formation temperature from 25 °C to 60 °C contribute little to the mordenite dispersion.

### 3.3. DSC study

$T_g$ is generally used as an indirect indicator to describe the flexibility of polymeric materials; the lower the $T_g$, the more flexible the material. DSC is the commonly used method for determination of chitosan's $T_g$ [49–51]. Herein, $T_g$ was determined by DSC in the second heating run to eliminate the influences of water and membrane processing [52,53]. The DSC trace of CS-25 membrane is presented in Fig. 3(a) and the $T_g$ is detected around 161 °C, which is in good agreement with Ahn's observation [54].

As we all know, plasticizers are additives used to increase the polymer flexibility. According to the free volume theory of plasticization, the plasticizer often works in a way of increasing free volume [55]. Accordingly, increased free volume leads to increased polymer chain flexibility and thus a reduction in $T_g$ [56]. Fig. 3(a) shows the DSC curves of pure CS membrane and sorbitol-plasticized CS membranes. The shift of $T_g$ toward lower temperatures with increase of sorbitol content indicates the increase of chitosan chain flexibility caused by sorbitol plasticization. The $T_g$ is lowered by ~11 °C than pure CS when 30 wt% sorbitol was added, and it is further lowered by another ~20 °C when the sorbitol content is increased to 40 wt%. However, when sorbitol content reached 40%, a second $T_g$ around 47.5 °C appeared as shown in Fig. 3(b). The second $T_g$ means the undesirable phase separation between chitosan and sorbitol [57–59]. Therefore, in order to increase chain flexibility as well as avoid phase separation, a sorbitol content of 30 wt% was selected in the subsequent investigations.

Fig. 4 shows the $T_g$ values of hybrid membranes. As a well documented phenomenon in literature [60–62], an increase of $T_g$ of hybrid membrane with increase of mordenite loading is distinctly represented. Sorbitol-plasticized hybrid membranes have lower $T_g$s than sorbitol-free membranes, and in addition, it seems that the plasticization effect of sorbitol becomes more pronounced at elevated temperature since CS/M(X)/S(30)-60 membranes show lower $T_g$s than CS/M(X)/S(30)-25 membranes, and the similar phenomena have been described by Arvanitoyannis et al. [46].

DSC measurements suggest that the addition of mordenite increase the rigidity of semi-rigid chitosan chain, resulting in increased stress during membrane formation, which in turn promotes chitosan rigidification. Only a single increased $T_g$ detected in all hybrid membrane samples reveals the overlap of rigidification regions around mordenite particles [19]. Sorbitol, the most efficient plasticizer of chitosan so far, served as a structural template during membrane preparation to increase the free volume in chitosan. This increased free volume leads to increased polymer chain flexibility and decreased stress as well as the subsequent decreased chitosan matrix rigidification. The plasticization becomes more pronounced at elevated temperature (60 °C) probably due to the increased polymer chain flexibility, thus hybrid membranes prepared at 60 °C are employed in the following sections to investigate the improvement of interfacial morphology.

### 3.4. XRD study

The XRD pattern of chitosan membrane shown in Fig. 5 confirms a partly crystalline structure of chitosan with three typical peaks at 11.8°, 18.8° and 22.6°, and the broad peak at around 20° is assigned to the amorphous phase. Similar results have been reported by Wang et al. [63] and Morni and Arof [64]. Typical diffraction peaks of mordenite at 9.7°, 13.4°, 23.2°, 25.6° and 27.7° are clearly observed in hybrid membranes as shown in Fig. 5.

Fig. 6 shows the change of chitosan crystallinity and overall crystallinity along with mordenite content in the presence or in the absence of sorbitol. The addition of crystalline mordenite particle interferes with the orderly packing of CS chains by both steric effect and forming hydrogen bonds between its surface –OH groups [65] and $–NH_2$ groups on CS, leading to the decrease of chitosan crystallinity and increase of overall crystallinity with the incorporation of amorphous sorbitol, both of chitosan crystallinity and overall crystallinity are decreased, due

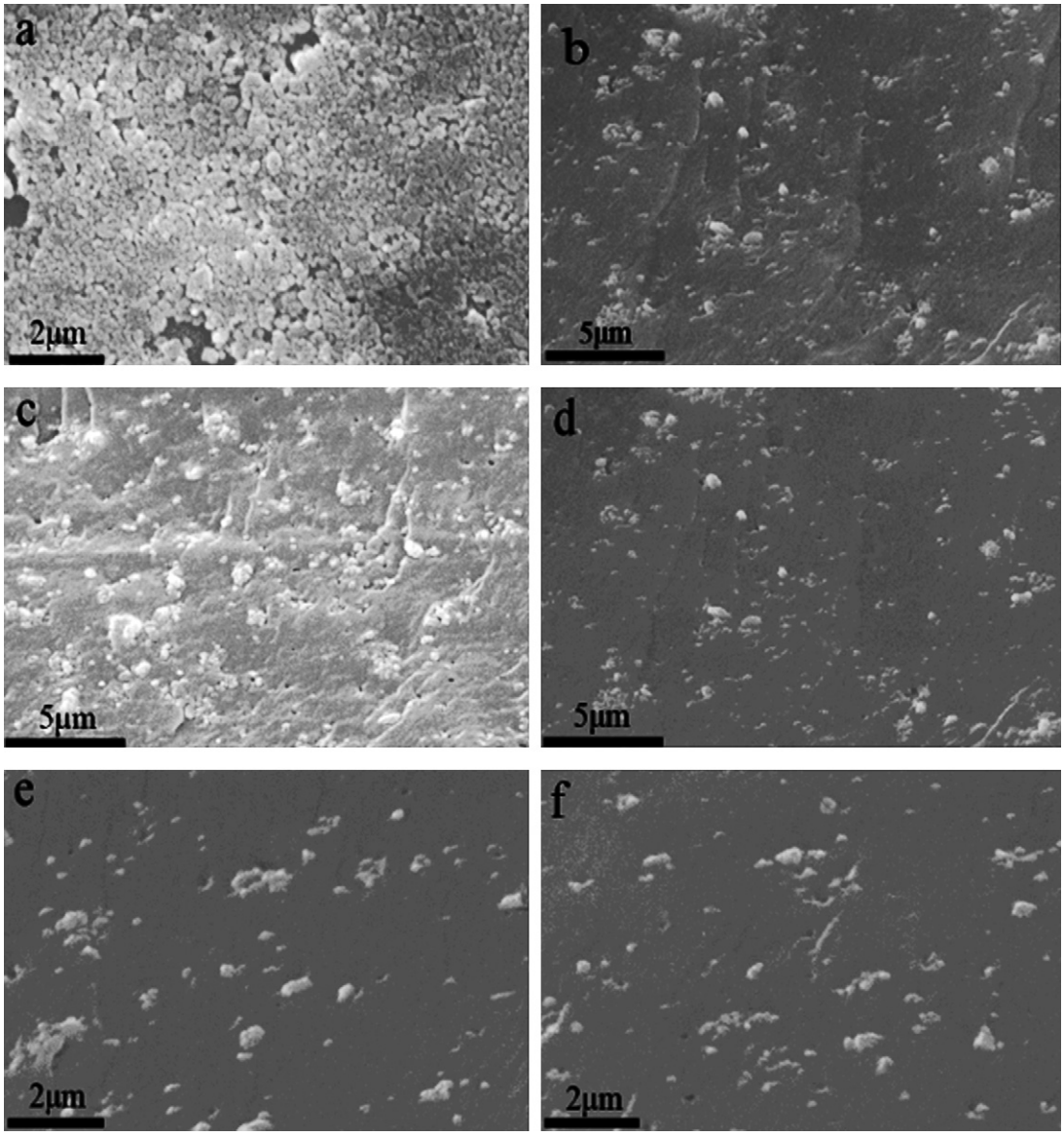


Fig. 2. Cross-section SEM images: (a) dispersed mordenite; (b) CS/M(15)-25; (c) CS/M(20)-25; (d and e) CS/M(15)/S(30)-25 on different scales; (f) CS/M(15)/S(30)-60.

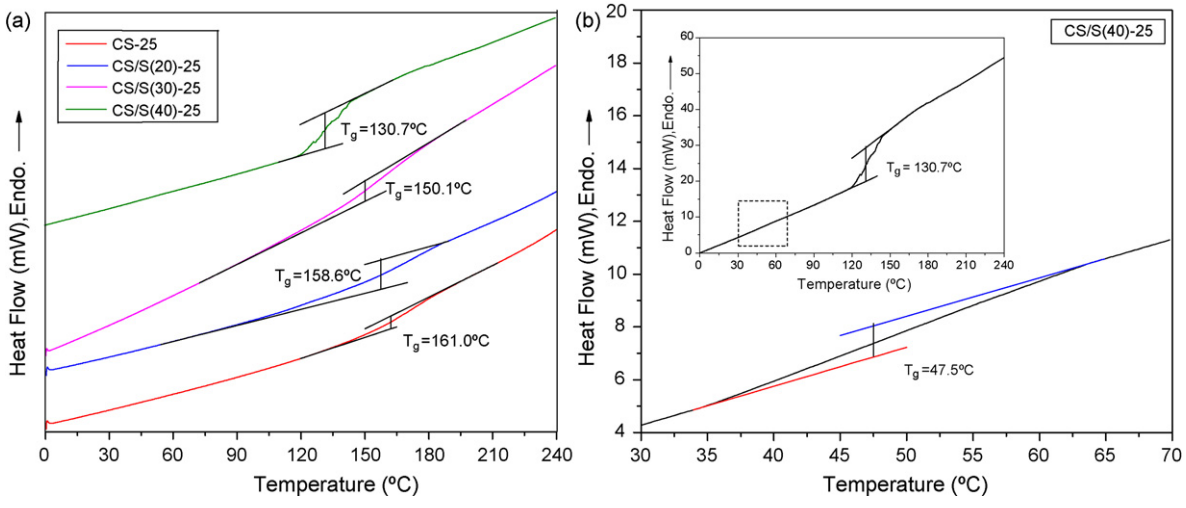


Fig. 3. DSC curves of (a) CS/S(Y)-25 membranes and (b) scale-up diagram of CS/S(40)-25 membrane.

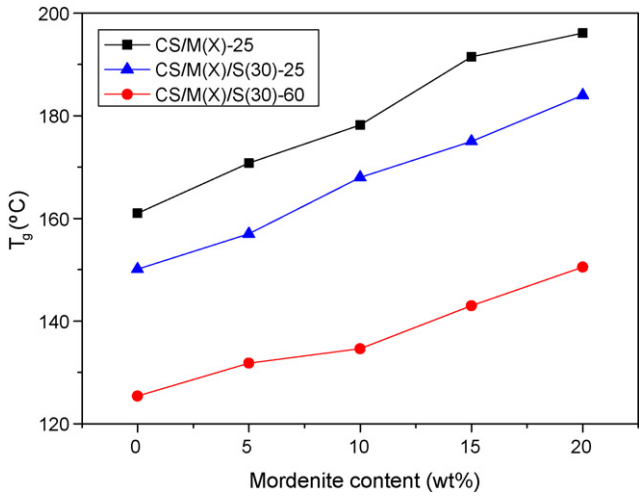


Fig. 4. $T_g$ values of CS/M(X)-25 and CS/M(X)/S(30)-T membranes.

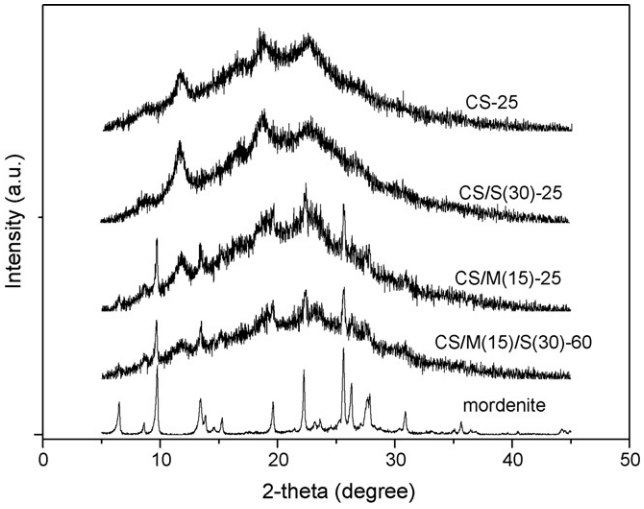


Fig. 5. XRD patterns of CS-25, CS/S (30)-25, CS/M (15)-25 and CS/M (15)/S (30)-60 membranes and mordenite.

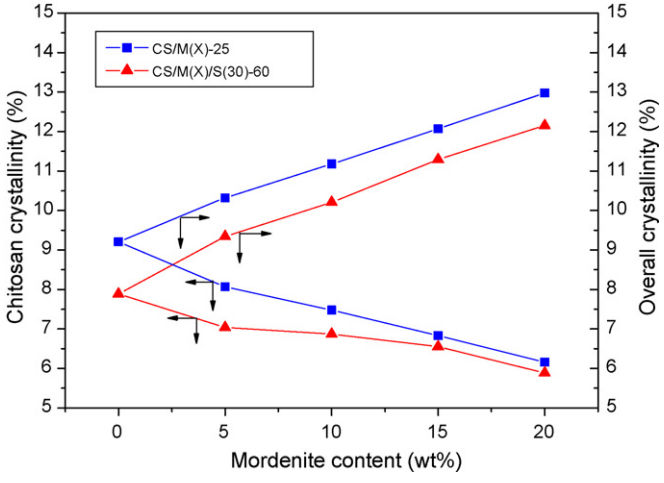


Fig. 6. Effects of mordenite content on chitosan crystallinity and overall crystallinity in CS/M(X)-25 and CS/M(X)/S (30)-60 membranes.

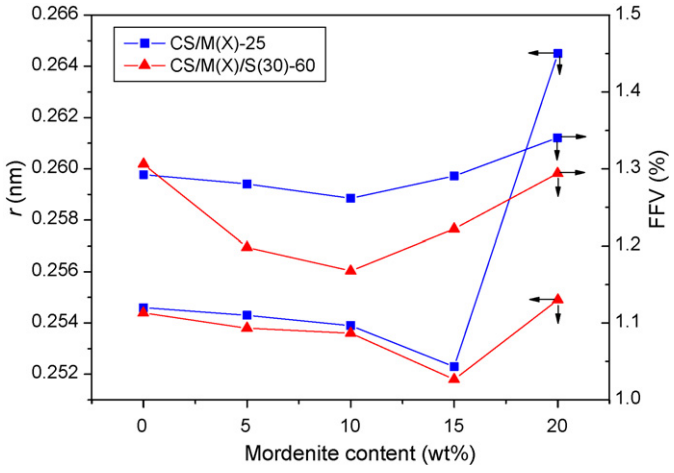


Fig. 7. Effects of mordenite content on the free volume properties of CS/M(X)-25 and CS/M(X)/S (30)-60 membranes.

to the hydrogen bonds formed between –OH groups on sorbitol and $–NH_2$ groups on CS during membrane preparation.

### 3.5. Free volume study

Numerous studies have revealed a strong correlation between PALS accessible free volume and separation properties of organic–inorganic hybrid membranes [66–69]. In a hybrid system, the free volume can be divided into three parts: free volume in the polymer matrix, that at the organic–inorganic interface and that in the inorganic phase. In the case of impermeable inorganic fillers, the last part may offer negligible contribution to the separation properties, which is the very case in this study. The membrane separation performances usually depend strongly on the size and concentration of free volume cavity, the larger and more these cavities are, the faster molecules transport through a membrane [67]. More specifically, free volume cavity size is crucial to selectivity between water and methanol.

Recently, PALS technique has been employed as a unique direct way to measure the free volume in membrane. In this technique, an o-positronium (o-Ps) particle is formed, which lifetime ($\tau$) is sensitive to the size ($r$-mean radius) and intensity ($I$) is related to the concentration (fractional free volume, FFV) of accessible free volume element cavity. The correlations are shown as follow, by assuming that the o-Ps is localized in a spherical potential well surrounded by an electron layer of thickness equal to 0.16 nm [70]. For most polymers, PALS spectra are described by a single o-Ps lifetime, $\tau_3$ and the corresponding $I_3$.

$$\tau = \frac{1}{2}\left[\frac{1-r}{r+\Delta r} + \frac{1}{2\pi}\sin\left(\frac{2\pi r}{r+\Delta r}\right)\right]^{-1} \qquad \mathrm{FFV} = \frac{4}{3\pi r^3 I}$$

The effects of mordenite and sorbitol on membrane free volume properties are illustrated in Fig. 7. As the mordenite content increased, both $r$ and FFV do not change consecutively. When the mordenite content is less than 15 wt%, chitosan rigidification is dominant and compressed chitosan chains in rigidification

region lead to free volume shrinkage, resulting in both reduction in $r$ and FFV. As mordenite concentration increases to 15 wt%, more and smaller voids are formed at the interface, which leads to the increased FFV and decreased $r$. The further increase of mordenite content to 20 wt% promotes the formation of more and larger interfacial voids, suggested by the SEM images together with the dramatic increases of $r$ and FFV. The addition of sorbitol brings a decrease in $r$ and an increase in FFV for CS-25 control membrane, decrease both in $r$ and FFV for CS/M(X)-25 membranes. The free volume property variations of CS-25 control membrane suggest sorbitol changes the CS chain packing which results in more and smaller voids between CS chains, and the increased FFV provides an evidence for the free volume theory of plasticization, and the shrinkage of free volume in CS/M(X)-25 membranes strongly reveals the minimization of interfacial voids by the addition of sorbitol.

In terms of methanol permeability, smaller free volume cavities are definitely expected, and chitosan rigidification is favorable, while non-selective interfacial voids should be avoided. With 15 wt% mordenite and 30 wt% sorbitol, the smallest free volume cavities are observed in CS/M(15)/S(30)-60 membrane, indicating an appropriate balance between chitosan rigidification and interfacial voids has been achieved.

### 3.6. Water/methanol uptake

As can be seen in Fig. 8, water uptake decreases with mordenite content, while a reversal behavior is observed for the methanol/water solution uptake, increased methanol uptake with mordenite content is thus reasonably inferred. This finding is primarily ascribed to the addition of the less hydrophilic mordenite compared with chitosan and sorbitol. Sorbitol, creating selective voids during membrane formation both in CS bulk matrix and at the interface, enables membrane with increased water affinity and methanol resistance. Moreover, an interesting phenomenon is observed in Fig. 8 that the liquid uptakes of CS/M(X)-25 and CS/M(X)/S(30)-60 membranes become much closer with the increase of mordenite content.

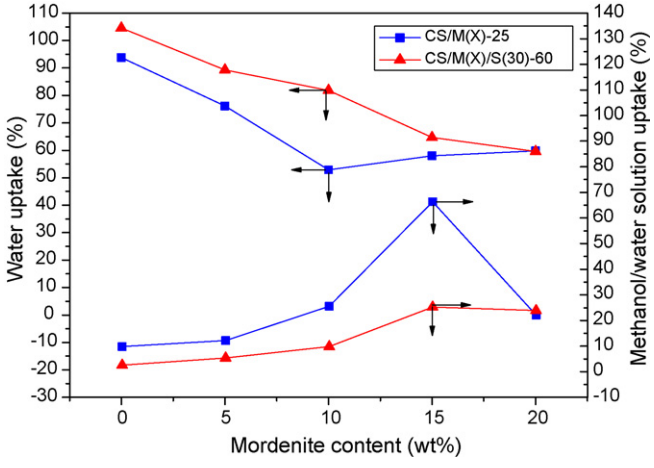


Fig. 8. Uptakes of CS/M(X)-25 and CS/M(X)/S (30)-60 membranes in water and 12 mol $L^{-1}$ methanol/water solution at 25 °C.

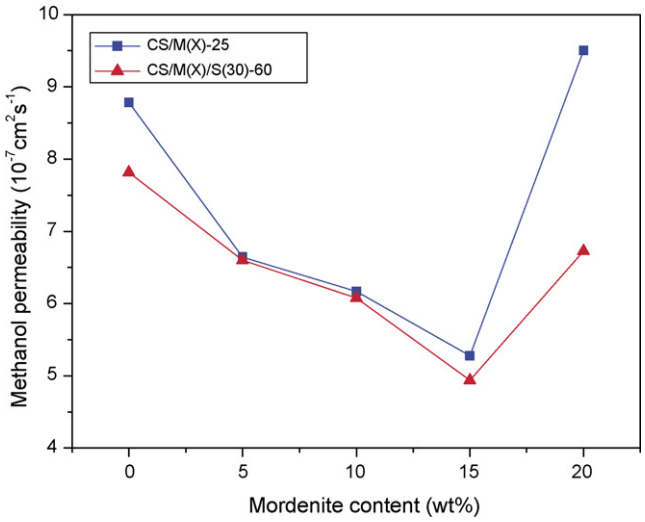


Fig. 9. Effects of mordenite content on methanol permeability of CS/M(X)-25 and CS/M(X)/S (30)-60 membranes in 12 mol $L^{-1}$ methanol/water solution at 25 °C.

### 3.7. Methanol permeability

Methanol permeation tests were performed to verify the correlation between interfacial morphology and methanol permeability of membranes and determine the optimum interfacial morphology ultimately. The methanol permeabilities of all membrane samples are presented in Fig. 9. Similar to the work of Mukoma et al. [71], CS-25 membrane shows a methanol permeability of $8.7 \times 10^{-7}$ cm$^2$ s$^{-1}$, as well as $7.8 \times 10^{-7}$ cm$^2$ s$^{-1}$, plasticized with 30 wt% sorbitol and $5.3 \times 10^{-7}$ cm$^2$ s$^{-1}$, incorporated with 15 wt% mordenite. CS/M(15)/S(30)-60 membrane displays the lowest methanol permeability, $4.9 \times 10^{-7}$ cm$^2$ s$^{-1}$, which is mainly attributed to the smallest free volume cavity size together with the enhanced methanol resistance.

The distinct similarity of curves in Figs. 7 and 9 reveals a close correlation between free volume cavity size and the methanol permeability of CS based membranes. It is reasonably assumed that tailoring interfacial morphology and pre-evaluating methanol permeability with free volume cavity size as indirect measurement would serve as a novel and facile methodology for organic–inorganic hybrid DMFC membrane investigation.

## 4. Conclusions

Incorporating plasticizer and increasing membrane formation temperature were jointly used to increase chain flexibility of the glassy polymer and reduce the stresses produced during solvent evaporation, and thereby delicately tailor the interfacial morphologies in organic–inorganic hybrid membranes for improved permeation property.

In the CS-based hybrid membranes, mordenite increased the rigidity of chitosan chain, leading to the formation of favorable chitosan rigidification and unfavorable interfacial voids. Sorbitol, as a template during membrane formation, decreased chitosan chain rigidity, and then suppressed both of

the non-selective interfacial voids and chitosan rigidification. This plasticization function was further enhanced by elevating formation temperature. The synergistic effect of 15 wt% mordenite, 30 wt% sorbitol as well as the membrane formation temperature of 60 °C endowed chitosan membrane with the optimum interfacial morphology in terms of methanol permeability, which was $4.9 \times 10^{-7}$ cm$^2$ s$^{-1}$ in 12 mol L$^{-1}$ methanol water solution at 25 °C. This value was 44% lower than that of pure chitosan control membrane and four times lower than that of Nafion 117 ($2.3 \times 10^{-6}$ cm$^2$ s$^{-1}$) membrane under the identical conditions [71]. Hopefully, this study will provide a simple and general way for the improvement of non-ideal organic–inorganic interfacial morphology and rational design of organic–inorganic hybrid materials; and in addition, a set of methodology for the facile evaluation of membrane permeation performance.

## Acknowledgements

We gratefully acknowledge financial support from the Cross-Century Talent Raising Program of Ministry of Education of China and the Program for Changjiang Scholars and Innovative Research Team in University from the Ministry of Education of China, and the Programme of Introducing Talents of Discipline to Universities (No: B06006).

## References

[1] N.W. DeLuca, Y.A. Elabd, J. Power Sources 163 (2006) 386–391.
[2] R. Wycisk, J. Chisholm, J. Lee, J. Lin, P.N. Pintauro, J. Power Sources 163 (2006) 9–17.
[3] C. Bailly, D.J. Williams, F.E. Karasz, W.J. MacKnight, Polymer 28 (1987) 1009–1016.
[4] G.P. Robertson, S.D. Mikhailenko, K. Wang, P. Xing, M.D. Guiver, S. Kaliaguine, J. Membr. Sci. 219 (2003) 113–121.
[5] S. Kaliaguine, S.D. Mikhailenko, K.P. Wang, P. Xing, G. Robertson, M. Guiver, Catal. Today 82 (2003) 213–222.
[6] R. Nolte, K. Ledjeff, M. Bauer, R. Mülhaupt, J. Membr. Sci. 83 (1993) 211–220.
[7] L. Jörissen, V. Gogel, J. Kerres, J. Garche, J. Power Sources 105 (2002) 267–273.
[8] Z. Chen, B. Holmberg, W. Li, X. Wang, W. Deng, R. Munoz, Y.S. Yan, Chem. Mater. 18 (2006) 5669–5675.
[9] H.T. Wang, B.A. Holmberg, L.M. Huang, Z.B. Wang, A. Mitra, J.M. Norbeck, Y.S. Yan, J. Mater. Chem. 12 (2002) 834–837.
[10] C.H. Rhee, H.K. Kim, H. Chang, J.S. Lee, Chem. Mater. 17 (2005) 1691–1697.
[11] B. Libby, W.H. Smyrl, E.L. Cussler, AIChE J. 49 (2003) 991–1001.
[12] S.H. Kwak, T.H. Yang, C.S. Kim, K.H. Yoon, Solid State Ionics 160 (2003) 309–315.
[13] C.Y. Chen, J.I. Garnica-Rodriguez, M.C. Duke, R.F.D. Costa, A.L. Dicks, J.C. Diniz da Costa, J. Power Sources 166 (2007) 324–330.
[14] L.N. Huang, L.C. Chen, T.L. Yu, H.L. Lin, J. Power Sources 161 (2006) 1096–1105.
[15] C. Guizard, A. Bac, M. Barboiu, N. Hovnanian, Sep. Purif. Technol. 25 (2001) 167–180.
[16] T.C. Merkel, B.D. Freeman, R.J. Spontak, Z. He, I. Pinnau, P. Meakin, A.J. Hill, Science 296 (2002) 519–522.
[17] T. Uragami, K. Okazaki, H. Matsugi, T. Miyata, Macromolecules 35 (2002) 9156–9163.
[18] K.J. Shea, D.A. Loy, Chem. Mater. 13 (2001) 3306–3319.
[19] T.T. Moore, W.J. Koros, J. Mol. Struct. 739 (2005) 87–98.
[20] W. Apichatachutapan, R.B. Moore, K.A. Mauritz, J. Appl. Polym. Sci. 62 (1996) 417–427.
[21] Q. Deng, R.B. Moore, K.A. Mauritz, J. Appl. Polym. Sci. 68 (1998) 747–763.
[22] P. Choi, N.H. Jalani, R.J. Datta, J. Electrochem. Soc. 152 (2005) A1548–A1554.
[23] M.L. Di Vona, D. Marani, C. D'Ottavi, M. Trombetta, E. Traversa, I. Beurroies, P. Knauth, S. Licoccia, Chem. Mater. 18 (2006) 69–75.
[24] Y.L. Liu, Y.H. Su, K.R. Lee, J.Y. Lai, J. Membr. Sci. 251 (2005) 233–238.
[25] Z.G. Shao, P. Joghee, I.M. Hsing, J. Membr. Sci. 229 (2004) 43–51.
[26] A.S. Aricò, V. Baglio, A. Di Blasi, P. Creti, P.L. Antonucci, V. Antonucci, Solid State Ionics 161 (2003) 251–265.
[27] S.D. Bhat, N.N. Mallikarjuna, T.M. Aminabhavi, J. Membr. Sci. 282 (2006) 473–483.
[28] F.B. Peng, Z.Y. Jiang, C.L. Hu, Y.Q. Wang, H.Q. Xu, J.Q. Liu, Sep. Purif. Technol. 48 (2006) 229–234.
[29] S.S. Kulkarni, S.M. Tambe, A.A. Kittur, J. Membr. Sci. 285 (2006) 420–431.
[30] R. Mahajan, R. Burns, M. Schaeffer, W.J. Koros, J. Appl. Polym. Sci. 86 (2002) 881–890.
[31] L.Y. Lu, H.L. Sun, F.B. Peng, Z.Y. Jiang, J. Membr. Sci. 281 (2006) 245–252.
[32] R. Mahajan, W.J. Koros, Ind. Eng. Chem. Res. 39 (2000) 2692–2696.
[33] H.J.C. te Hennepe, D. Bargeman, M.H.V. Mulder, C.A. Smolders, J. Membr. Sci. 35 (1987) 39–55.
[34] T.T. Moore, Effects of Materials, Processing and Operating Conditions on the Morphology and Gas Transport Properties of Mixed Matrix Membranes, Department of Chemical Engineering, University of Texas, Austin, TX, USA, 2004, p. 312.
[35] Y. Li, T.S. Chung, C. Cao, S. Kulprathipanja, J. Membr. Sci. 260 (2005) 45–55.
[36] Y. Li, H.M. Guan, T.S. Chung, S. Kulprathipanja, J. Membr. Sci. 275 (2006) 17–28.
[37] M. Ghazali, M. Nawawi, R.Y.M. Huang, J. Membr. Sci. 124 (1997) 53–62.
[38] J.J. Shieh, R.Y.M. Huang, J. Membr. Sci. 127 (1997) 185–202.
[39] Y. Wan, K.A.M. Creber, B. Peppley, V.T. Bui, J. Appl. Polym. Sci. 89 (2003) 306–317.
[40] P. Mukoma, B.R. Jooste, H.C.M. Vosloo, J. Power Sources 136 (2004) 16–23;
J. Coronas, J. Santamaria, Separ. Purif. Method 28 (1999) 127–177.
[41] B. Smitha, S. Sridhar, A.A. Khan, J. Power Sources 159 (2006) 846–854;
J. Kjaer, J. Yale-Andersen, N.A. Knudsen, Solid State Ionics 46 (1991) 169–173.
[42] N. Rao, T.P. Andersen, P. Ge, Solid State Ionics 72 (1994) 334–337.
[43] Y. Tsujimi, M. Kobayashi, T. Yagi, Phys. B 263-264 (1999) 310–312.
[44] N. Suyatma, L. Tighzert, A. Copinet, V. Coma, J. Agric. Food Chem. 53 (2005) 3950–3957.
[45] I.S. Arvanitoyannis, I. Kolokuris, A. Nakayama, N. Yamamoto, S.I. Aiba, Carbohyd. Polym. 34 (1997) 9–19.
[46] I.S. Arvanitoyannis, A. Nakayama, S.I. Aiba, Carbohyd. Polym. 37 (1998) 371–382.
[47] A. Lazaridou, C.G. Biliaderis, Carbohyd. Polym. 48 (2002) 179–190.
[48] I. Salla, T. Montanari, P. Salagre, Y. Cesteros, G. Busca, J. Phys. Chem. B 109 (2005) 915–922.
[49] Y.M. Dong, Y.H. Ruan, H.W. Wang, Y.G. Zhao, D.X. Bi, J. Appl. Polym. Sci. 93 (2004) 1553–1558.
[50] K. Sakurai, T. Maegawa, T. Takahashi, Polymer 41 (2000) 7051–7056.
[51] M. Mucha, A. Pawlak, Thermochim. Acta 427 (2005) 69–76.
[52] M. Zhang, X.H. Li, Y.D. Gong, N.M. Zhao, X.F. Zhang, Biomaterials 23 (2002) 2641–2648.
[53] R.C. Baltieri, L.H. Innocentini Mei, J. Bartoli, Macromol. Symp. 197 (2003) 33–44.
[54] J.S. Ahn, H.K. Choi, C.S. Cho, Biomaterials 22 (2001) 923–928.
[55] L. Di Gioia, S. Guilbert, J. Agric. Food Chem. 47 (1999) 1254–1261.
[56] R.J. Hill, Ind. Eng. Chem. Res. 45 (2006) 6890–6898.
[57] M.T. Kalichevsky, J.M.V. Blanshard, Carbohyd. Polym. 20 (1993) 107–113.
[58] M.T. Kalichevsky, E.M. Jaroszkiewicz, J.M.V. Blanshard, Int. J. Biol. Macromol. 14 (1992) 257–266.

[59] M.T. Kalichevsky, J.M.V. Blanshard, P.E. Tokarczuk, Int. J. Food Sci. Technol. 28 (1993) 139–151.
[60] P.S. Theocaris, G.D. Spathis, J. Appl. Polym. Sci. 27 (1982) 3019–3025.
[61] X.Y. Shang, Z.K. Zhu, J. Yin, X.D. Ma, Chem. Mater. 14 (2002) 71–77.
[62] M. Moaddeb, W.J. Koros, J. Membr. Sci. 125 (1997) 143–163.
[63] S.F. Wang, L. Shen, Y.J. Tong, L. Chen, I.Y. Phang, P.Q. Lim, T.X. Liu, Polym. Degrad. Stabil. 90 (2005) 123–131.
[64] N.M. Morni, A.K. Arof, J. Power Sources 77 (1999) 42–48.
[65] T.J. Dines, L.D. MacGregor, C.H. Rochester, Spectrochim. Acta A 59 (2003) 3205–3217.
[66] G. Monserrat, J. Barsema, R.E. Galindo, D. Cangialosi, J. Garcia-Turiel, W.E. van Zyl, H. Verweij, D.H.A. Blank, Polym. Eng. Sci. 44 (2004) 1240–1246.
[67] T.C. Merkel, B.D. Freeman, R.J. Spontak, Z. He, I. Pinnau, P. Meakin, A.J. Hill, Chem. Mater. 15 (2003) 109–123.
[68] T.C. Merkel, Z. He, I. Pinnau, B.D. Freeman, P. Meakin, A.J. Hill, Macromolecules 36 (2003) 6844–6855.
[69] F.B. Peng, L.Y. Lu, H.L. Sun, Y.Q. Wang, J.Q. Liu, Z.Y. Jiang, Chem. Mater. 17 (2005) 6790–6796.
[70] S.J. Tao, J. Chem. Phys. 56 (1972) 5499–5510.
[71] P. Mukoma, B.R. Jooste, H.C.M. Vosloo, J. Membr. Sci. 243 (2004) 293–299.